TiO 2 nanocolumn arrays for more efficient and stable perovskite solar cells

Zhelu Hu, José Miguel García-Martín, Yajuan Li, Laurent Billot, Baoquan Sun, Fernando Fresno, Antonio García-Martín, María Ujué González, Lionel Aigouy, Zhuoying Chen

TiO_2 nanocolumn arrays for more efficient and stable perovskite solar cells

Zhelu Hu,[a] José Miguel García-Martín,[b] Yajuan Li,[c] Laurent Billot,[a] Baoquan Sun,[c] Fernando Fresno,[d] Antonio García-Martín,[b] María Ujué González,[b] Lionel Aigouy,[a] Zhuoying Chen[a]*

a. LPEM, ESPCI Paris, PSL Research University, Sorbonne Université, CNRS, 10 Rue Vauquelin, F-75005 Paris, France

b. Instituto de Micro y Nanotecnología IMN-CNM, CSIC, CEI UAM+CSIC, Isaac Newton 8, E-28760 Tres Cantos, Madrid, Spain

c. Institute of Functional Nano & Soft Materials (FUNSOM), Jiangsu Key Laboratory for Carbon-Based Functional Materials & Devices, Soochow University, 199 Ren'ai Road, Suzhou, 215123, Jiangsu, PR China

d. Photoactivated Processes Unit, IMDEA Energy Institute, Avda. Ramón de la Sagra, 3, 28935 Móstoles, Madrid, Spain.

* Corresponding author. E-mail: zhuoying.chen@espci.fr

KEYWORDS: TiO_2 arrays, hybrid perovskite, solar cells, electron transport layer, light harvesting, light concentration

ABSTRACT. Organic-inorganic hybrid perovskite solar cells have attracted much attention due to their high power conversion efficiency (＞25%) and low-cost fabrication. Yet improvements are still needed for more stable and more performing solar cells. In this work, a series of TiO_2 nanocolumn photonic structures has been intentionally fabricated on half of the compact TiO_2-coated fluorine-doped tin oxide substrate by glancing angle deposition with magnetron sputtering, a method particularly suitable for industrial applications due to its high reliability and reduced cost when coating large areas. These vertically aligned nanocolumn arrays were then applied as the electron transport layer (ETL) into triple-cation lead halide perovskite solar cells based on $Cs_{0.05}(FA_{0.83}MA_{0.17})_{0.95}Pb(I_{0.83}Br_{0.17})_3$. By comparison to solar cells built onto the same substrate without nanocolumns, the use of TiO_2 nanocolumns can significantly enhance the power conversion efficiency of the perovskite solar cells by 7 % and prolong their shelf life. Here, the detailed characterizations on the morphology and the spectroscopic aspects of the nanocolumns, their near-field and far-field optical properties, solar cells characteristics, as well as the charge transport properties, provide mechanistic insights on how 1D TiO_2 nanocolumns affect the performance of perovskite halide solar cells in terms of the charge transport, light-harvesting, and stability, knowledge necessary for the future design of more-performing and more-stable perovskite solar cells.

INTRODUCTION

During the last decade, hybrid organometal halide perovskite solar cells (PSCs) have drawn sustained intensive attention, mainly due to their outstanding photovoltaic behavior and their low-cost solution fabrication.[1–5] While their stability is still to be improved,[6–9] the power conversion efficiency (PCE) of the state-of-the-art PSCs has been certificated exceeded 25%, which presents a great potential to compete with the traditional commercial silicon solar cells.[10] A typical PSC architecture consists of three components, including a perovskite absorber layer, sandwiched between an electron transport layer (ETL) and a hole transport layers (HTL), all of which co-determine the final performance of a PSC. Concerning ETLs, their critical roles are to transport photogenerated electrons and at the same time to block holes from the perovskite absorber. In order to achieve high power conversion efficiency, the electron collection must be efficient otherwise severe carrier recombination can occur at the ETL/perovskite interface.[3] So far, ETLs based on various semiconductor metal oxides (such as TiO_2, ZnO, SnO_2 ...) and *n*-type molecules have been investigated in PSCs to optimize the ETL/perovskite interface, as well as the improve the growth of perovskite layer.[1,11–13]

By comparison to the planar ETLs, mesoporous ETLs appear to be more advantageous for perovskite solar cells to achieve higher efficiency, higher stability, and less hysteresis.[3,14] For example, mesoporous scaffolds can be formed by depositing TiO_2 nanoparticles, which transport electrons while providing a large ratio of surface area for the nucleation of perovskite absorber.[3] Nevertheless, such straightforward TiO_2 nanoparticle-based scaffolds have some drawbacks such as the existence of numerous grain boundaries/structural defects, difficulty of pore-filling by the perovskite precursor, and perturbation to the growth of perovskite grains.[15–17] As a result, compromised charge transport efficiency and severe charge recombination at the perovskite/ETL

interface was observed.[18] By comparison, well-oriented one-dimension (1-D) TiO_2 nanorods/nanowires/nanotubes arrays represent a promising strategy,[14,18–30] exhibiting less surface defects and grain boundaries and facilitating precursor pore-filling. 1D TiO_2 arrays can thus provide a direct physical conductive paths to extract and transport efficiently carriers generated by the perovskite layer. In terms of synthetic methods, 1D TiO_2 arrays for perovskite solar cells have been demonstrated through anodization,[23,26,29] block-copolymer template,[30] and solvothermal methods.[14,18–20,24,25,27,28] While the majority of these studies focused on the electronic contribution of the TiO_2 nanoarrays in perovskite solar cells (in terms of charge transport and carrier recombination), their optical contribution has not been well-characterized. While some studies observed the enhanced perovskite solar cell stability associated with the application of TiO_2 1D arrays,[14,21–23,27] the origins of such observations remain unclear. In addition, one of the important issues in this field concerns how to compare fairly the devices with the 1D array inserted and the devices without. The additional fabrication steps involved to generate the 1D arrays can introduce some source of differences between the device containing 1D arrays and the device without. Together with the possible batch-to-batch solar cell fabrication differences, it is therefore not straightforward to attribute the observed enhancement in solar cell characteristics directly to the inserted 1D arrays.

In terms of light-harvesting strategies, various nanostructures have been proposed for perovskite solar cells including textured absorber layer,[31,32] textured substrates,[33,34] SiO_2 prism arrays,[35] polymer micolens,[36] indium tin oxide (ITO) nanocone arrays,[37] metallic plasmonic nanoparticles,[38,39] microstructure composite hole transport layer,[40] TiO_2 nanoparticles,[41] and TiO_2 nano-dome and nano-void arrays.[42] While many of these studies focused only on simulations and optical measurements,[36,37,42] experimental studies applying textures,[31–34] SiO_2 prisms,[35] metallic plasmonic nanoparticles,[38,39] microstructure composites,[40] and TiO_2 nanoparticles[41] have indeed

demonstrated functional and more performing perovskite solar cells owning to such light-harvesting strategies. By comparison to the popular metallic plasmonic structures, non-metal materials with high permittivity are alternative choices for nanoantenna enhancing the optical absorption and fluorescence processes at their surroundings.[43–45] In particular, TiO_2 nanostructures such as nanodisks, owing to their large refractive index, have been shown to localize light and enhance the fluorescence of a nearby fluorescent nanoparticle.[46] In the context of perovskite solar cells, due to the absence of optical absorption in the visible spectrum and its excellent electron transporting properties, 1D TiO_2 nanoarrays should be an excellent electronic and optical booster.

In this work, vertically aligned 1D TiO_2 nanocolumn arrays are intentionally fabricated onto half of the compact TiO_2-coated fluorine-doped tin oxide (FTO) substrates by the glancing angle deposition (GLAD), a method capable to generate well-oriented inorganic nanorods with uniform dimensions on substrates when using physical vapor deposition (PVD).[21,47–49] Although the most common PVD technique in the scientific literature to perform GLAD is thermal evaporation, from an applied point of view the most interesting one is magnetron sputtering (MS), which is widely used in many industrial applications due to its high reliability and reduced cost when coating large areas.[50,51] Thus, our approach to fabricate the aligned 1D TiO_2 nanocolumn arrays is GLAD with magnetron sputtering. Structural, spectroscopy and optical characterizations were then performed on these TiO_2 nanoarrays by comparison to the compact TiO_2 (cp-TiO_2) counterpart of the same substrate. In particular, by near-field optical microscopy (SNOM), the light-management capability of these nanoarrays is studied in detail, revealing strong concentration of electromagnetic fields at the surroundings of the nanoarrays. Functional triple-cation lead perovskite halide solar cells based on $Cs_{0.05}(FA_{0.83}MA_{0.17})_{0.95}Pb(I_{0.83}Br_{0.17})_3$ are then built onto the above-mentioned substrates, half of which covered by TiO_2 nanocolumn electron transport layer (ETL) and the other half covered by cp-TiO_2 ETL. By comparison to the solar cells built on only a planar cp-TiO_2 ETL of the same

FTO substrate, solar cells with TiO_2 nanocolumn arrays exhibit a 5% increase in its short-circuit current and a 7% enhancement in its power conversion efficiency, together with a significantly prolonged shelf-life. Revealed by electrochemical impedance spectroscopy, the application of TiO_2 nanocolumn arrays leads to a lower charge transport resistance and a higher charge recombination resistance in the solar cell, both contributing to the observed enhanced photovoltaic performance. In addition, such TiO_2 nanocolumn arrays exhibit a more significant optical absorption in the UV spectrum by comparison to the planar counterpart, capable to perform partial UV-screening boosting the stability of the perovskite solar cell. The combined structural, spectroscopic, photovoltaic and optical characterizations presented herein provide a detail analysis on the physical origins of the beneficial roles of 1D TiO_2 nanocolumn arrays in hybrid perovskite solar cells.

RESULTS AND DISCUSSION

The TiO_2 nanocolumn arrays obtained by glancing angle deposition composed of dense TiO_2 nanocolumns uniformly aligned perpendicular to the substrate (**Figure 1**). These nanocolumns exhibit an average diameter of 89 ± 18 nm and an average length of 254 ± 27 nm. For hole-blocking purpose, a thin layer of cp-TiO_2 ETL with a thickness of about 50 nm was applied before the deposition of the TiO_2 nanocolumn arrays onto half of the substrate surface. No observable change on the morphology nor on the RMS roughness of the FTO and the cp-TiO_2 ETL was induced by fabrication process of the TiO_2 nanocolumn arrays (Figure. S1 and S2 of the supporting information). Despite the distinctively different microstructure of the nanocolumn sample by comparison to the cp-TiO_2 sample, the perovskite layers deposited on top of both samples exhibit similar morphology, grain size and surface roughness (Figure 1d and e, Figure S3). Cross-sectional SEM characterizations showed clearly the different sub-layers on both the control (without

nanocolumns) and the nanocolumn sample (Figure 1f and g). The perovskite thin film deposited on top of the cp-TiO_2 layer exhibited a thickness of about 450 nm. By comparison, the perovskite thin film deposited on top of the nanocolumns is slightly thinner, reaching about 350 nm in thickness. Nevertheless, as shown in the cross-sectional SEM image, the perovskite precursor solution infiltrates well in between the nanocolumns forming a dense layer of perovskite in tight contact with each nanocolumn. This is coherent with a previous study on tilted 1D TiO_2 nanocolumn arrays prepared by GLAD but with thermal evaporation where excellent infiltration of the perovskite was also achieved.[22] Combining the infiltrated part and the part above the nanocolumns, there was likely a more important amount of perovskite crystallites on the nanocolumn sample compared to the planar sample.

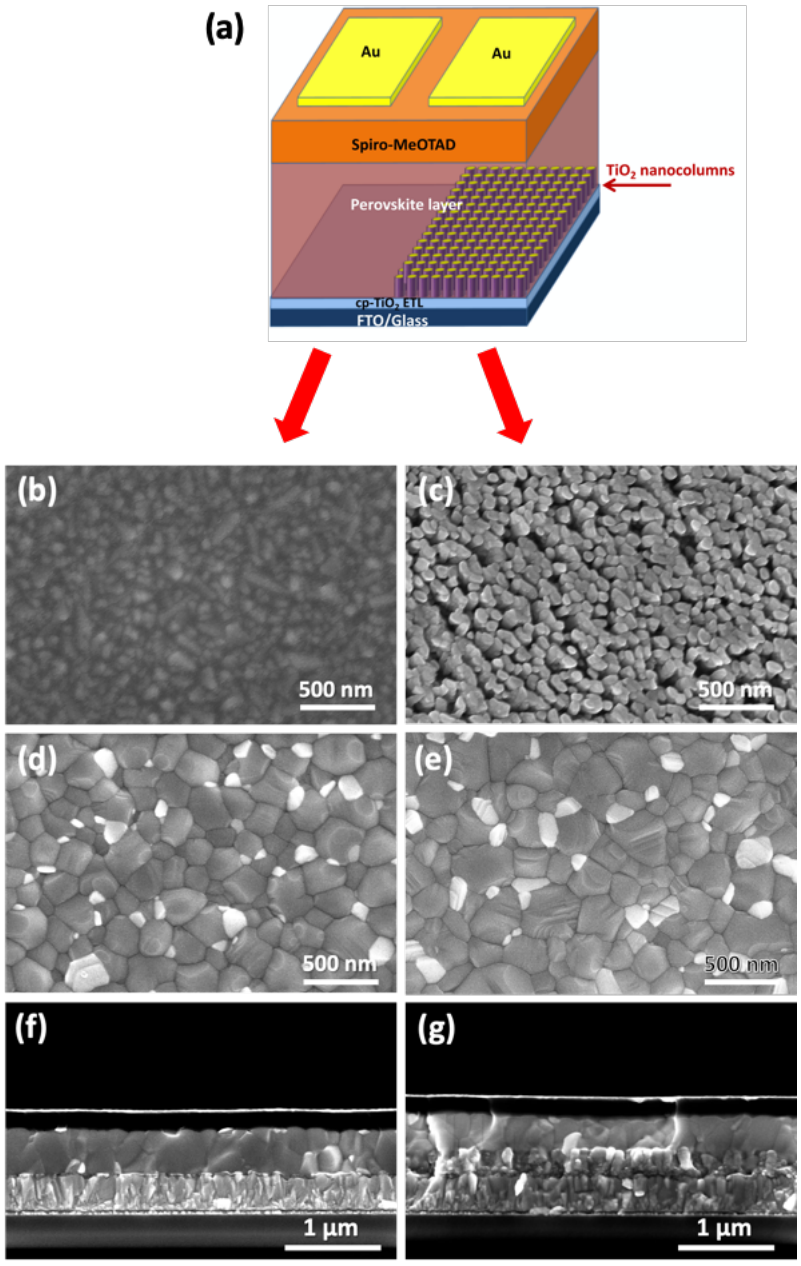

Figure 1. (a) Schematics of the perovskite solar cell architecture with half of its interface covered by cp-TiO_2 ETL and the other half covered by TiO_2 nanocolumn arrays; (b, c) Top-view scanning electron microscopy (SEM) images of the cp-TiO_2 layer (b) and the TiO_2 nanocolumn arrays (c); (d, e) The SEM image of the perovskite film deposited on a cp-TiO_2 ETL (d) and on TiO_2 nanocolumn arrays (e); (f, g) Cross-sectional SEM image after the deposition of hole-transport

polymer on the part of the sample with only a cp-TiO_2 ETL (without nanocolumns, f) and the part of the sample with TiO_2 nanocolumn arrays (g).

X-ray photoelectron spectroscopy (XPS) was applied to compare the surface chemistry of the nanocolumn array part and the planar cp-TiO_2 (control) part of the sample (**Fig. 2**). As shown in Fig. 2a, for the nanocolumn arrays, the doublet of Ti $2p_{3/2}$ and Ti $2p_{1/2}$ arising from the spin orbit-splitting are located at binding energies of 465.2 and 459.4 eV, respectively. Almost identical Ti 2p peaks were observed on the control part of the sample except for a 0.2 eV shift to lower binding energy. The binding energies and the shapes of these Ti 2p peaks are consistent with Ti^{4+} in a TiO_2 lattice.[52] The O 1s spectrum from both sample areas are also very similar (Fig. 2b). For the nanocolumn arrays, it can be fitted with two peaks at binding energy of 530.7 and 532.2 eV, attributed to the lattice oxygen in TiO_2 and non-lattice oxygen species (such as -OH groups and/or oxygen vacancies),[53,54] respectively. Nearly identical O 1s spectrum was found on the control cp-TiO_2 area except also for a 0.2 eV shift to lower binding energy. Such a 0.2 eV shift in binding energy was observed in the C 1s spectrum recorded from the two sample areas. Combining the similar peak shape/position of Ti 2p and O 1s spectra observed, we conclude that the surface chemistry of both the nanocolumn arrays and the cp-TiO_2 are nearly identical even though a slight difference of conductivity may exist between them leading to the small shift of binding energy observed.

After the deposition of the perovskite absorber layer onto one of the above-mentioned substrates, the substrate was cut into half separating the nanocolumn part and the cp-TiO_2 part in order to perform XRD characterizations. The perovskite films deposited on both the nanocolumn arrays and on the control cp-TiO_2 exhibited strong Bragg diffraction peaks which can be indexed

according to the $Cs_{0.05}(FA_{0.83}MA_{0.17})_{0.95}Pb(I_{0.83}Br_{0.17})_3$ "black" (α) perovskite phase,[55] while more intense diffractions were observed on the perovskite/nanocolumn sample (Fig. 2c). This is coherent with the SEM observation, likely due to infiltration of perovskite precursor solution in between the nanocolumns leading to the existence of more perovskite crystallites on the nanocolumns compared to the control planar cp-TiO_2. In addition, by comparison to the planar TiO_2, the nanocolumns may offer more nucleation sites facilitating perovskite crystallization. Such observation is similar as those previously observed on other mesoporous ETLs.[2,3] Diffraction peak corresponding to the (001) diffraction of PbI_2 was also observed on both samples. This is due to the 10% mole excess of PbI_2 from the perovskite precursor solution. Here, an excess of PbI_2 was intentionally added into the perovskite precursor solution to optimize the solar cell performance according to previous reports to passivate the grain boundary of the mixed cation perovskite films aiming to benefit the charge transport and to reduce charge recombination.[56,57] The UV-Vis optical absorbance spectra on these perovskite films revealed an about 1.3-fold increase of optical absorption on the nanocolumns compared to the perovskite film deposited on the control planar cp-TiO_2 (Figure 2d). Such an increase of optical absorbance can be a direct consequence of the more perovskite materials deposited on the nanocolumns due to precursor infiltration as well as the light harvesting effect of the nanocolumns (which will be discussed below).

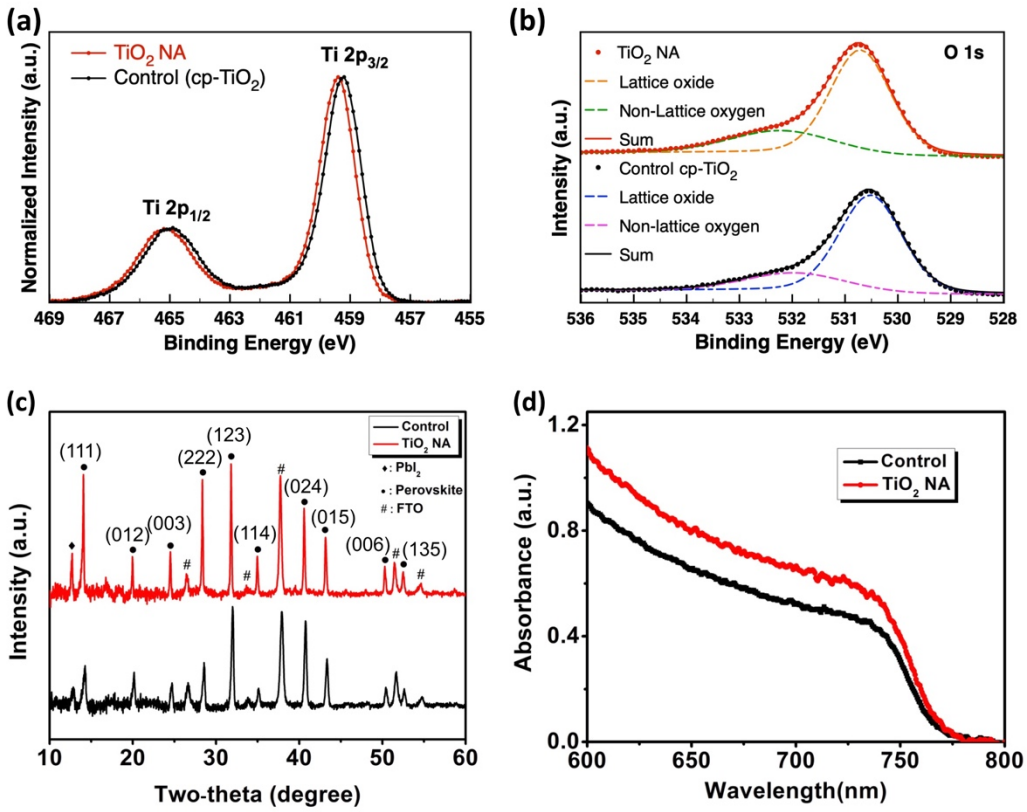

Figure 2. (a) XPS spectra of Ti 2p regions of the TiO_2 nanocolumn (NA) sample and the planar cp-TiO_2 (control) sample; (b) XPS spectra of O 1s regions of the TiO_2 NA sample and control sample. Dash lines represent the fits and solid lines represent the sums of the two fitted peaks; (c) X-ray diffraction (XRD) patterns and (d) the absorbance spectra of the perovskite film deposited on cp-TiO_2/FTO glass substrate and on TiO_2 NA/cp-TiO_2/FTO glass substrate, respectively.

Scanning near-field optical microscopy (SNOM) was applied to characterize the potential light-harvesting capability of TiO_2 nanocolumns for their application in a perovskite solar cell. When combined with a fluorescence nanoparticle, SNOM has been widely used to characterize biological samples and optoelectronic devices,[58–60] capable to reveal the distribution of electromagnetic fields at the vicinity of a nano-object/nanostructure. Here a fluorescent nanoparticle was used to probe

the surface of the TiO_2 nanocolumns by comparison to the planar cp-TiO_2 part situated on the same substrate. The measured fluorescence intensity of such a nanoparticle at a specific sample position can thus indicate the intensity of the local electromagnetic field. The schematic of the current SNOM experiment is shown in **Figure 3**. During the SNOM experiment, a sharp tungsten atomic force microscope (AFM) tungsten tip on which an upconversion fluorescent nanoparticle is glued is scanned above the illuminated sample. The nanoparticle absorbs the near-field at the laser wavelength (λ = 650 nm) and re-emits it in the green-yellowish spectral zone (λ = 520-550 nm). The sample was illuminated in a transmission mode, from its rear face. By scanning the tip (with the nanoparticle) over the TiO_2 sample surface and simultaneously recording fluorescence signal at each scan position, both a topographic map of the sample and a map of the upconversion fluorescence (at λ = 550 nm) from the nanoparticle can be obtained. In order to keep the same measurement condition without any alteration of the probe, all the scanning experiments were performed with the same AFM tip.

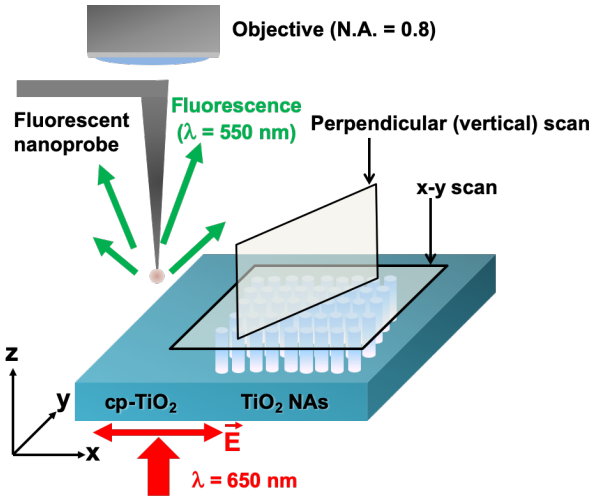

Figure 3. Schematic of the illumination configuration and the scanning mode of the current scanning near-field optical microscopy (SNOM) experiments. TiO_2 nanocolumns (NAs) were

fabricated onto half of the cp-TiO_2-coated FTO substrate surface so that AFM/SNOM measurements on the surface of TiO_2 nanocolumns and on cp-TiO_2 can be performed on the same substrate.

From the AFM topography mapping presented in Figure 4a and 4d, both surfaces of the cp-TiO_2 and TiO_2 nanocolumn arrays are very homogeneous, providing a uniform area for the growth of perovskite materials. In contrast to the topography mapping, the fluorescence mappings obtained on them revealed distinctively different features (Figure 4b and 4e). Comparing to the two fluorescence mapping figures, one can observe on the surface of TiO_2 nanocolumns more inhomogeneity of the fluorescence signal from the nanoparticle glued on the AFM tip, indicating strong variations and a localization of electromagnetic field on the nanocolumn surface. In order to visualize the effect of the TiO_2 nanocolumns on the modulation of the incident light, two randomly selected line profiles from the fluorescence mapping obtained on the cp-TiO_2 and the TiO_2 nanocolumns were exhibited in Figure 4c and 4f. Comparing these line profiles, one can observe enormous variations of the fluorescence intensity on TiO_2 nanocolumns by comparison to the planar cp-TiO_2. This indicates that TiO_2 nanocolumns perturb the incident field and create zones on which light is strongly enhanced compared to others. A vertical fluorescence scan in the out-of-plane direction was performed from the surface of TiO_2 nanocolumns to 1 μm above the surface (Figure 4g). The intensity of fluorescence is strongest with a clear in-plane modulation when the AFM tip and the glued fluorescent nanoparticle are close to the surface of the TiO_2 nanocolumns. By comparison, when the distance between the tip and the nanocolumns increases, the observed fluorescence signal becomes weaker together with less in-plane modulation, indicating a smaller and less localized electromagnetic field when the AFM probe is far away from the TiO_2 nanocolumns. Similar as the above observed enhanced fluorescence process, in a

perovskite solar cell configuration, the existence of TiO_2 nanocolumns and their resultant localization of electromagnetic field can lead to a more efficient light absorption by the perovskite absorber around the nanocolumns, leading to more photons available to be converted to electrons.

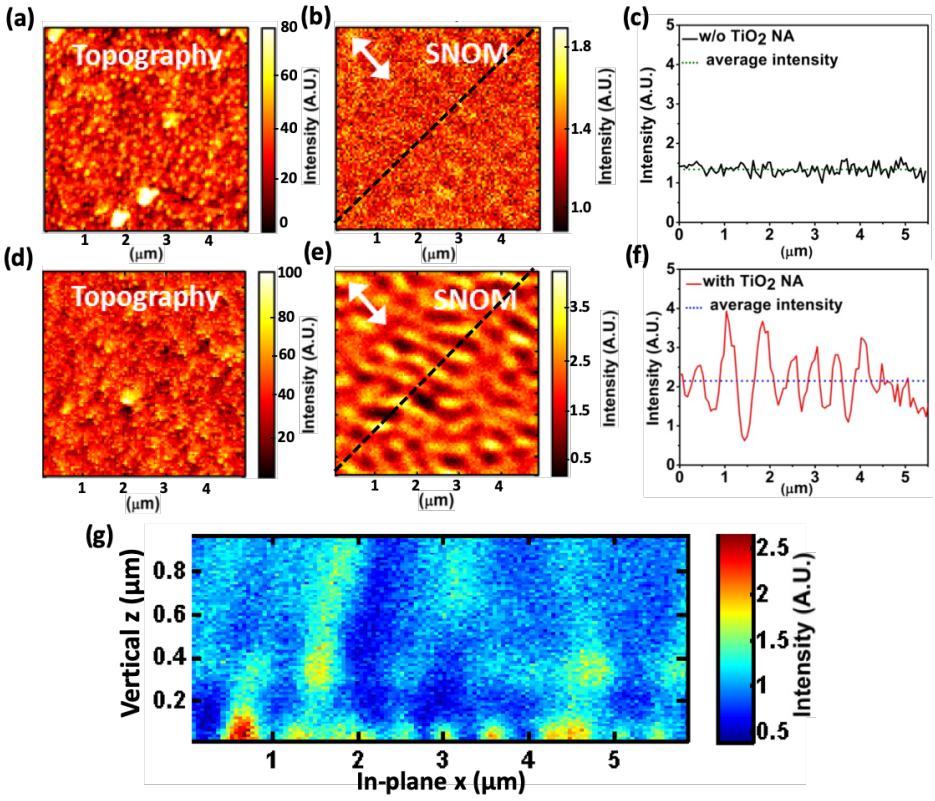

Figure 4. AFM topography of planar cp-TiO_2 (a) and TiO_2 nanocolumns (NA) (d). Fluorescence maps of cp-TiO_2 layer (b) and TiO_2 NA (d). (c) and (f) exhibit the line profiles of the fluorescence map obtained on cp-TiO_2 (black dash line shown in (b)) and on TiO_2 NAs (black dash line shown in (e)). (g) The vertical fluorescence map obtained from the surface of TiO_2 NAs to 1 μm above the surface.

Functional perovskite solar cells were fabricated on both TiO_2 nanocolumn ETL and planar cp-TiO_2 ETL located on the same FTO substrate according to the device architectures shown in Figure 1. The current-voltage (*J-V*) characteristics, measured under 100 mW cm^{-2} AM 1.5G simulated

illumination, of the best-performing perovskite solar cells from the same FTO substrate are shown in Figure 5a. By comparison to the perovskite solar cell built on a planar cp-TiO_2 ETL, the incorporation of TiO_2 nanocolumn ETL leads to a slight increase of the solar cell short circuit photocurrent density (J_{sc}), from 19.27 mA/cm^2 to 20.19 mA/cm^2, and the fill-factor (FF), from 73.59% to 75.14%. The combination of both lead to an about 7% increase in the power conversion efficiency (PCE) in the solar cell with nanocolumns compared to the one with only a planar cp-TiO_2 ETL. The photovoltaic characteristics of these perovskite solar cells built onto the *same* substrate are listed in **Table 1** (the standard distribution of photovoltaic performance measured on different substrates were presented in **Table S1**). Their external quantum efficiencies (EQEs) are shown in Figure 5b. The short-circuit current densities for the solar cell built on cp-TiO_2 ETL and on TiO_2 nanocolumns obtained from integrating their EQE spectra with the AM 1.5G spectrum are 19.10 and 20.03 mA/cm^2, respectively, which are in agreement with the J_{sc} measured in the *J-V* curves. The observation that the solar cell with TiO_2 nanocolumns shows a higher EQE value in the wavelength range of 450-600 nm than that of the cell without TiO_2 nanocolumns is qualitatively coherent with the optical absorbance spectra of the perovskite film deposited onto these substrates (Figure S4). The larger observed J_{sc} on the solar cell built on TiO_2 nanocolumns is coherent with the results obtained by SEM, UV-Vis absorption and SNOM. It is likely a combined consequence from both more perovskite materials deposited on top of the TiO_2 nanocolumns and the light-concentration effects of the TiO_2 nanocolumns.

Electrochemical impedance spectroscopy (EIS) was performed onto these solar cells to probe the charge transfer and recombination process at the interface between the ETL and perovskite absorber. Figure 5c shows the Nyquist plots of the two perovskite solar cells built on the cp-TiO_2 ETL and the TiO_2 nanocolumn ETL of the same FTO substrate, measured in dark with an external bias holding at their respective V_{oc} and in the frequency range from 20 Hz to 2 MHz. The obtained

EIS spectra can be fitted well with the equivalent electrical circuit model commonly used on perovskite solar cells.[61,62] The equivalent circuit is shown in the inset of Figure 5c and the inner series resistance (R_s), charge transport resistance (R_{tr}), and the recombination resistance (R_{rec}) obtained from fitting are listed in Table 1. The whole set of fitting parameters are listed in the supporting information **Table S2**. When the nanocolumn ETL was applied, the charge transport resistance R_{tr} was reduced from 20 Ω to 13.5 Ω and the recombination resistance was substantially increased from 2085 Ω to 4410 Ω. Coherent with the enhanced fill-factor observed in the *J-V* characteristics, the current EIS results indicated that charge transport is more efficient in the TiO_2 nanocolumn ETL compared to the cp-TiO_2 ETL and the carrier recombination is less severe in the former case. These results suggest that, besides the optical benefits mentioned above, by comparison to the planar cp-TiO_2, TiO_2 nanocolumn ETL exhibits electronic benefits in terms of charge transport and recombination suppression.

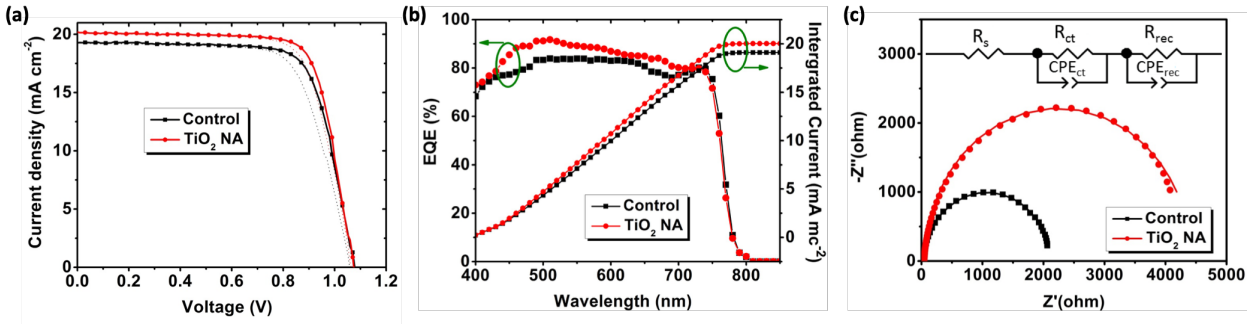

Fig. 5. (a) Current density-voltage (J-V) photovoltaic characteristics measured on the perovskite solar cells built on a cp-TiO_2 ETL (control) and on TiO_2 nanocolumn (NA) ETL of the same FTO substrate, under 100 mW cm^{-2} AM 1.5G illumination. Solid dots and lines indicate results from the reverse voltage scan (from V_{oc} to 0 V) and dotted lines indicate results from forward voltage scan (from 0 V to V_{oc}). (b) The EQE spectra for the perovskite solar cells shown in (a) and the

corresponding integrated J_{sc} of the devices. (c) The typical Nyquist plots (symbols) obtained from the perovskite solar cells shown in (a) tested in dark and at their V_{oc}. Solid lines represent the fits obtained by applying the equivalent circuit shown in the inset.

Table 1. The summary of the photovoltaic characteristics of the perovskite solar cells built on a cp-TiO_2 ETL (control) and on TiO_2 nanocolumn (NA) ETL of the same FTO substrate. Results are presented together with the parameters (inner series resistance R_s, charge transport resistance R_{tr}, and recombination resistance R_{rec}) obtained from fitting the electrochemical impedance spectroscopy results. J_{sc}: short-circuit current density; V_{oc}: open-circuit voltage; *FF*: fill-factor; *PCE*: power-conversion efficiency.

ETL	J_{sc} (mA/cm^2)	V_{oc} (V)	*FF* (%)	*PCE* (%)	R_s (Ω)	R_{tr} (Ω)	R_{rec} (Ω)
cp-TiO_2	19.27	1.08	73.59	15.31	10.05	20.02	2085
TiO_2 NA	20.19	1.08	75.14	16.38	10.08	13.52	4410

In addition to the above-mentioned optical and electrical benefits, it was observed that the application of TiO_2 nanocolumns significantly enhanced the shelf life of these perovskite solar cells. **Figure 6a** presents the normalized PCE of the unencapsulated perovskite solar cells built on a cp-TiO_2 ETL and on a TiO_2 nanocolumn ETL of the same FTO substrate as a function of the storage time. When stored in argon, the perovskite solar cell built on TiO_2 nanocolumns maintained ~ 93.6 % of its initial PCE value after 126 days of storage, whereas under identical conditions the perovskite solar cell built on cp-TiO_2 exhibited only ~ 80.5 % of its original PCE. When stored in air (with ~ 11% of humidity), the solar cell with the application of TiO_2 nanocolumns maintained ~ 75.3 % of

its initial PCE value after 91 days of storage, which represents a more than 3.8-fold enhancement by comparison to the solar cell without nanocolumns (on cp-TiO_2) that maintained only ~ 19.8 % of its initial PCE under the same conditions. Under constant UV illumination, the perovskite solar cells built on TiO_2 nanocolumns also showed superior stability by comparison to the one built on the cp-TiO_2 ETL of the same substrate (**Figure S5**). After 95 hours of constant UV illumination (3 mW cm^{-2}) at λ = 365 nm in argon atmosphere, the perovskite solar cell with nanocolumns still maintained 92.4% of its initial PCE while the one without nanocolumns exhibited only 50.1% of its initial PCE. As observed from their optical images (inset of Figure 6a), after 91 days of air storage, there was inhomogeneous color with plenty of transparent spots visible as well as a transparent area surrounding the edge of the top electrode on the perovskite solar cell without nanocolumns, suggesting perovskite absorber decomposition. This is in clear contrast with the perovskite solar cell built on nanocolumns from the same substrate, where homogeneous perovskite absorber was still observed in the optical image. These observations are similar to the enhanced perovskite solar cell stability reported in previous studies with the application of 1D TiO_2 arrays,[14,23] while the physical origins accounting for the enhanced stability remain not well understood. To shed light on this, we compared the optical absorption from an identical area (by placing an aperture with a transmission diameter of 6 mm) between three sample conditions: a bare FTO/glass substrate, a cp-TiO_2-coated area on a FTO/glass substrate, and a TiO_2 nanocolumn-coated area on the same above-mentioned cp-TiO_2-coated FTO/glass substrate. As shown in Figure 6b (black symbols), the optical absorption contributed from the planar cp-TiO_2 is very small due to its limited thickness (50 nm). By comparison, the optical absorption contribution from the TiO_2 nanocolumns is much more significant (red symbols, Figure 6b), in particular in the wavelength range between 300 nm and 370 nm. Such optical absorption in the UV spectrum from the TiO_2

nanocolumns is thus beneficial for perovskite solar cells minimizing UV degradation occurred during each *J-V* measurements. While a much thicker cp-TiO_2 planar ETL should in principle be able to achieve the similar optical contribution as TiO_2 nanocolumns in the UV spectrum, a thicker cp-TiO_2 film may lead to a significantly increased solar cell series resistance, worse charge transport properties, and more carrier recombination events. These results underlined the unique advantages of TiO_2 nanocolumns in perovskite solar cells, capable to perform partial UV screening without scarifying the electronic properties of ETL.

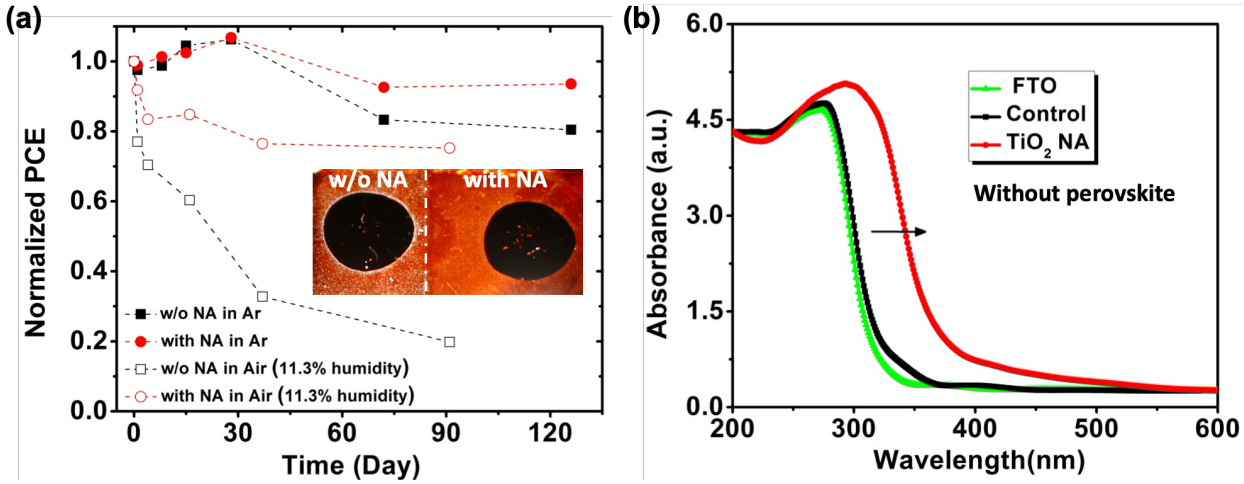

Fig. 6 (a) The evolution of power conversion efficiency (PCE) of perovskite solar cells with and without TiO_2 nanocolumn (NA) ETL built on the same FTO substrate over storage time. These solar cells were stored either in argon or in air (humidity at 11.3%), at 25 °C in dark. Insets exhibit the optical images of the area around the top electrode of the two solar cells built on the same FTO substrate after 91 days of degradation in air. The white dash line indicates the separation between the NA-coated part and part without NAs. The diameter of these top electrodes is 3.55 mm. (b) The comparison of optical absorption before perovskite deposition from an identical area (by placing a 6-mm-diameter aperture) from: a bare FTO/glass

substrate (FTO), a cp-TiO_2-coated area on a FTO/glass substrate (control condition), and a TiO_2 NA-coated area from the same cp-TiO_2-coated FTO/glass substrate as the control condition.

CONCLUSION

In summary, vertically-aligned 1-D TiO_2 nanocolumn arrays were realized by glancing angle deposition and they were subsequently applied as the ETL to fabricate functional triple-cation lead perovskite halide solar cells based on $Cs_{0.05}(FA_{0.83}MA_{0.17})_{0.95}Pb(I_{0.83}Br_{0.17})_3$. By comparison to solar cells built on planar cp-TiO_2 of the same FTO substrate, solar cells built on a TiO_2 nanocolumn ETL exhibit a 5% increase of short-circuit current and a 7% enhancement in its power conversion efficiency together with a significantly prolonged shelf-life. Various macroscopic and microscopic characterization methods were combined to identify the physical origins of the observed enhanced photovoltaic property. Identified from SEM characterization, SNOM, and UV-vis absorption, TiO_2 nanocolumn ETL led to enhanced perovskite optical absorption, higher solar cell short-circuit currents, and better device stability by providing numerous precursor infiltration paths, near-field light concentration, and partial UV screening. In addition to these optical advantages, electrochemical EIS analysis showed that TiO_2 nanocolumn ETL is also superior to planar cp-TiO_2 in terms of charge transport and the reduction of recombination losses. These findings thus provide mechanistic insights on how 1D TiO_2 nanocolumns affect the performance of perovskite halide solar cells in terms of the charge transport, light-harvesting, and stability, knowledge necessary for the future design of more-performing and more-stable perovskite solar cells.

METHODS

The preparation of TiO_2 nanocolumn arrays. The aligned 1D TiO_2 nanocolumn arrays have been fabricated in two steps. The first step was the fabrication of Ti nanocolumns by GLAD with magnetron sputtering using the setup and methodology described in detail in a previous work.[63] The sputter gas was argon and the parameters used were: pressure = 0.15 Pa, power (DC discharge) = 300 W, and tilt angle between substrate and target = 75º. The second step is the thermal oxidation of the Ti nanocolumn arrays to obtain TiO_2 nanocolumns. For this purpose, they were placed in a quartz tube inside a tubular furnace. Synthetic air was passed through the tube at a flowrate of 50 $cm^3\ min^{-1}$. The furnace was then heated with a 10 °C min^{-1} ramp up to 500 ºC and kept at that temperature for 10 min, after which it was let to cool down naturally. The transformation was characterized by XRD and by AFM and SEM imaging before and after the process. The metallic Ti became fully oxidized after the thermal treatment, mainly into the TiO_2 rutile phase (Figure S6 in the Supporting Information). While the nanocolumns are broadened by comparison to the initial as-deposited Ti ones (Figure S7), the columnar array structure is maintained.

The fabrication of perovskite solar cells. FTO-coated glass substrates were cleaned by four sequential ultrasonication baths in 2% hallmanex detergent solution, deionized water, acetone and isopropanol for 15 min each. Blow-dried substrates were then further cleaned by oxygen plasma for 10 minutes. For the deposition of a cp-TiO_2 ETL, a sol-gel precursor solution derived from titanium (IV) isopropoxide[64] was spin-coated at 4000 rpm onto cleaned FTO substrates. A substrate corner was intentionally left un-covered by cp-TiO_2 exposing the bare FTO underneath. These substrates were then annealed in an oven in air first at 120 °C for 15 minutes and subsequently at 450 °C for 1 hour. TiO_2 nanocolumn arrays were fabricated by the methods mentioned above onto half of the cp-TiO_2-coated substrate by intentionally masking the other half of the substrate in order to discard any additional source of differences between the device containing nanocolumns and the

device without nanocolumns. The mixed cation perovskite $Cs_{0.05}(FA_{0.83}MA_{0.17})_{0.95}Pb(I_{0.83}Br_{0.17})_3$ layer was then deposited from their precursor solution by one-step spin-coating onto the above-mentioned substrate, with TiO_2 nanoarrays on half of its surface and cp-TiO_2 ETL on another half of its surface (as a control condition). To prepare the solution precursor for the $Cs_{0.05}(FA_{0.83}MA_{0.17})_{0.95}Pb(I_{0.83}Br_{0.17})_3$ perovskite layer, formamidinium iodide (FAI) and methylammonium bromide (MABr) are synthesized according to previous works.[65,66] Lead iodide (PbI_2), lead bromide ($PbBr_2$) and cesium iodide (CsI) were purchased from Sigma Aldrich. A precursor solution was formed by dissolving FAI (1 M), MABr (0.2 M), PbI_2 (1.1 M), and $PbBr_2$ (0.2 M) in a solvent mixture of dimethylformamide (DMF) and dimethyl sulfoxide (DMSO) (4:1, v/v) according to a previous report.[67] In parallel, a stock solution containing 1.5 M of CsI dissolved in DMSO was prepared. CsI stock solution was then added into the above-mentioned precursor solution to achieve the desired composition in the final precursor solution. The deposition of the perovskite precursor solution onto TiO_2-coated FTO was performed in an Ar-filled glovebox by two-step spin-coating first at 1000 rpm for 10 s and then at 5000 rpm for 45 s. During the second spin-coating step, 100 µl chlorobenzene was dropped on the spinning substrate after 30 s of spinning. After spin-coating the perovskite films were annealed inside the glovebox at 100 °C for 60 min on a hot-plate. The precursor solution of the hole-transport layer (HTL) was prepared by dissolving 72.3 mg Spiro-OMeTAD (Sigma Aldrich), 17.5 µl Li-bis(trifluoromethanesulfonyl) imide (Sigma Aldrich, 520 mg/mL in acetonitrile) and 28.8 µl tert-butylpyridine (Sigma Aldrich) were into 1 mL chlorobenzene. This HTL solution was then spin-coated on top of the perovskite layer at 4000 rpm for 30 s. Finally, 100-nm-thick gold top contacts were thermally evaporated on the surface of the Spiro-OMeTAD HTL to complete the solar cell structure.

Structural and optical characterizations. Scanning near-field optical microscopy (SNOM) measurements were performed by a homemade near-field optical microscope that uses a

fluorescent nanocrystal as a near-field detector.[68,69] Excitation was performed with an internally modulated laser diode ($\lambda \cong 650$ nm, $f_{mod} = 320$ Hz) in a transmission mode at normal incidence. The collection of the near-field signal was performed using a wide numerical aperture objective (Olympus LMPlanFl 100x 0.8) and sent to a photomultiplier tube and to a lock-in amplifier (EG&G Instruments Model 7260DSP). The sample was set on a piezo-electric 3D stage (Nanocube, Physik Instrumente) for scanning. Scanning electron microscopy (SEM) characterizations were performed by a FEI Magellan 400 system with a standard field emission gun source. Powder X-ray diffraction (XRD) spectra were obtained by a PANalytical X'Pert X-ray diffractometer using Cu-K_α radiation. For perovskite-coated samples, UV-Visible absorbance spectra were recorded on an about 1-mm-diameter sample spot in a transmission mode by an Ocean Optics HL-2000 fiber-coupled tungsten halogen lamp and an Ocean Optics HR4000 spectrometer (200-1100 nm). 3 different sample spots on the same substrate area (the part with nanocolumns or the part without nanocolumns) were verified to ensure the reproducibility of the absorbance spectra. For the FTO/cp-TiO_2 substrate with nanocolumns covered on its half (without perovskite coating), optical absorbance spectra were recorded in a transmission mode by a V-770ST UV/VIS/NIR spectrometer with a mask (diameter of aperture = 6 mm) allowing optical transmission in only the area of interest. X-ray photoelectron spectroscopy (XPS) measurement was carried out by a KRATOS AXIS Ultra DLD apparatus at a base pressure of 3×10^{-9} Torr (X-ray Source: AlKα). Atomic Force Microscopy (AFM) was performed using a Dimension Icon from Bruker operating in non-contact mode with high-resolution probes (radius: 2nm) from Next-Tip.

Photovoltaic Characterizations. Solar cell current-voltage characteristics were measured in an Ar-filled glovebox by a computer-controlled Keithley 2612B source measurement unit (SMU). Devices were illuminated through the transparent substrate (FTO/glass) side by a class ABB (ASTM E927-10) Newport LCS-100 solar simulator with an AM 1.5G filter operated at 1 SUN.

The light intensity was first calibrated by a calibrated Si reference solar cell (ReRa Solutions B.V.). For the external quantum efficiency (EQE) measurements, a monochromatic light beam was obtained from a white light source and an Oriel Cornerstone monochromator with appropriate order sorting filters. The monochromatic illumination was calibrated by a NIST-calibrated Si photodiode. The solar cell short-circuit current I_{sc} (A) at each monochromatic wavelength was measured in air by a Keithley 2634B SMU. The EQE spectrum was determined by $EQE(\%) = \frac{I_{sc}(A)}{P(W)} \times \frac{1240}{\lambda(nm)} \times 100$ where P (W) is the power of the monochromatic illumination. The electrochemical impedance spectroscopy (EIS) measurements were performed in electrochemical workstation (Agilent, E4980A) under dark and with an external applied bias holding at the open-circuit voltage of the solar cell. The frequency range of the EIS measurements was from 20 Hz to 2 MHz with a modulation amplitude of 20 mV.

ASSOCIATED CONTENT

Supporting Information. The Supporting Information is available free of charge on the ACS Publications website (PDF). Morphology characterizations on the surface of compact-TiO_2 (cp-TiO_2) and bare FTO before and after the nanocolumn fabrication procedure and thermal treatment; AFM characterizations of the perovskite layer on cp-TiO_2 and on TiO_2 nanocolumns; The optical absorbance spectra of the perovskite film; UV degradation behaviors of perovskite solar cells built on TiO_2 nanocolumns and on cp-TiO_2 ETL; XRD and SEM characterizations of TiO_2 nanocolumns from Ti nanocolumn arrays by thermal oxidation; Photovoltaic parameters with standard distribution of the perovskite solar cells built onto different substrates; EIS parameters for the perovskite solar cells with TiO_2 nanocolumn ETL and cp-TiO_2 ETL.

AUTHOR INFORMATION

Corresponding Author

*zhuoying.chen@espci.fr

Author Contributions

The manuscript was written through contributions of all authors. All authors have given approval to the final version of the manuscript.

Notes

The authors declare no competing financial interest.

ACKNOWLEDGMENT

We thank the Programme Decouverte Chine 2019 (project 43619UM) financed by the MEAE (Le ministère de l'Europe et des Affaires étrangères) and the PROCES project (ANR-17-CEO5-0028-01) and from the CNRS and the CSIC through the Spanish-French program PICS (grant SolarNano #PICS07687 and #PIC2016FR2). Z. H. acknowledge the China Scholarship Council for PhD scholarship. We also acknowledge the service from the MiNa Laboratory at IMN, which is funded from CM (project S2018/NMT-4291 TEC2SPACE), MINECO (project CSIC13-4E-1794) and EU (FEDER, FSE).

REFERENCES

(1) Liu, M.; Johnston, M. B.; Snaith, H. J. Efficient Planar Heterojunction Perovskite Solar Cells by Vapour Deposition. *Nature* **2013**, *501*, 395–398.

(2) Bera, A.; Sheikh, A. D.; Haque, M. A.; Bose, R.; Alarousu, E.; Mohammed, O. F.; Wu, T.

Fast Crystallization and Improved Stability of Perovskite Solar Cells with Zn 2 SnO 4 Electron Transporting Layer: Interface Matters. *ACS Appl. Mater. Interfaces* **2015**, *7*, 28404–28411.

(3) Haque, M. A.; Sheikh, A. D.; Guan, X.; Wu, T. Metal Oxides as Efficient Charge Transporters in Perovskite Solar Cells. *Adv. Energy Mater.* **2017**, *7*, 1602803.

(4) Sheikh, A. D.; Munir, R.; Haque, M. A.; Bera, A.; Hu, W.; Shaikh, P.; Amassian, A.; Wu, T. Effects of High Temperature and Thermal Cycling on the Performance of Perovskite Solar Cells: Acceleration of Charge Recombination and Deterioration of Charge Extraction. *ACS Appl. Mater. Interfaces* **2017**, *9*, 35018–35029.

(5) Ansari, F.; Salavati-Niasari, M.; Nazari, P.; Mir, N.; Ahmadi, V.; Abdollahi Nejand, B. Long-Term Durability of Bromide-Incorporated Perovskite Solar Cells via a Modified Vapor-Assisted Solution Process. *ACS Appl. Energy Mater.* **2018**, *1* (11), 6018–6026.

(6) Rivkin, B.; Fassl, P.; Sun, Q.; Taylor, A. D.; Chen, Z.; Vaynzof, Y. Effect of Ion Migration-Induced Electrode Degradation on the Operational Stability of Perovskite Solar Cells. *ACS Omega* **2018**, *3* (8), 10042–10047.

(7) Zhang, J.; Luo, H.; Xie, W.; Lin, X.; Hou, X.; Zhou, J.; Huang, S.; Ou-Yang, W.; Sun, Z.; Chen, X. Efficient and Ultraviolet Durable Planar Perovskite Solar Cells via a Ferrocenecarboxylic Acid Modified Nickel Oxide Hole Transport Layer. *Nanoscale* **2018**, *10* (12), 5617–5625.

(8) Hou, X.; Pan, L.; Huang, S.; Wei, O.-Y.; Chen, X. Enhanced Efficiency and Stability of Perovskite Solar Cells Using Porous Hierarchical TiO 2 Nanostructures of Scattered

Distribution as Scaffold. *Electrochim. Acta* **2017**, *236*, 351–358.

(9) Luo, H.; Lin, X.; Hou, X.; Pan, L.; Huang, S.; Chen, X. Efficient and Air-Stable Planar Perovskite Solar Cells Formed on Graphene-Oxide-Modified PEDOT:PSS Hole Transport Layer. *Nano-Micro Lett.* **2017**, *9*, 39.

(10) Green, M. A.; Dunlop, E. D.; Levi, D. H.; Hohl-Ebinger, J.; Yoshita, M.; Ho-Baillie, A. W. Y. Solar Cell Efficiency Tables (Version 54). *Prog. Photovoltaics Res. Appl.* **2019**, *27*, 565–575.

(11) Bai, Y.; Yu, H.; Zhu, Z.; Jiang, K.; Zhang, T.; Zhao, N.; Yang, S.; Yan, H. High Performance Inverted Structure Perovskite Solar Cells Based on a PCBM:Polystyrene Blend Electron Transport Layer. *J. Mater. Chem. A* **2015**, *3*, 9098–9102.

(12) Jiang, Q.; Zhang, L.; Wang, H.; Yang, X.; Meng, J.; Liu, H.; Yin, Z.; Wu, J.; Zhang, X.; You, J. Enhanced Electron Extraction Using SnO2 for High-Efficiency Planar-Structure HC(NH2)2PbI3-Based Perovskite Solar Cells. *Nat. Energy* **2017**, *2* (1), 16177.

(13) Liu, D.; Kelly, T. L. Perovskite Solar Cells with a Planar Heterojunction Structure Prepared Using Room-Temperature Solution Processing Techniques. *Nat. Photonics* **2014**, *8*, 133–138.

(14) Fakharuddin, A.; Di Giacomo, F.; Palma, A. L.; Matteocci, F.; Ahmed, I.; Razza, S.; D'Epifanio, A.; Licoccia, S.; Ismail, J.; Di Carlo, A.; Brown, T. M.; Jose, R. Vertical TiO2 Nanorods as a Medium for Durable and High Efficiency Perovskite Solar Modules. *ACS Nano* **2015**, *9* (8), 8420–8429.

(15) Wei, D.; Ji, J.; Song, D.; Li, M.; Cui, P.; Li, Y.; Mbengue, J. M.; Zhou, W.; Ning, Z.; Park,

N.-G. A TiO 2 Embedded Structure for Perovskite Solar Cells with Anomalous Grain Growth and Effective Electron Extraction. *J. Mater. Chem. A* **2017**, *5*, 1406–1414.

(16) Grancini, G.; Marras, S.; Prato, M.; Giannini, C.; Quarti, C.; De Angelis, F.; De Bastiani, M.; Eperon, G. E.; Snaith, H. J.; Manna, L.; Petrozza, A. The Impact of the Crystallization Processes on the Structural and Optical Properties of Hybrid Perovskite Films for Photovoltaics. *J. Phys. Chem. Lett.* **2014**, *5*, 3836–3842.

(17) Giordano, F.; Abate, A.; Correa Baena, J. P.; Saliba, M.; Matsui, T.; Im, S. H.; Zakeeruddin, S. M.; Nazeeruddin, M. K.; Hagfeldt, A.; Graetzel, M. Enhanced Electronic Properties in Mesoporous TiO2 via Lithium Doping for High-Efficiency Perovskite Solar Cells. *Nat. Commun.* **2016**, *7*, 1–6.

(18) Wu, W. Q.; Chen, D.; Cheng, Y. B.; Caruso, R. A. Three-Dimensional Titanium Oxide Nanoarrays for Perovskite Photovoltaics: Surface Engineering for Cascade Charge Extraction and Beneficial Surface Passivation. *Sustain. Energy Fuels* **2017**, *1* (9), 1960–1967.

(19) Zhong, D.; Cai, B.; Wang, X.; Yang, Z.; Xing, Y.; Miao, S.; Zhang, W.-H.; Li, C. Synthesis of Oriented TiO2 Nanocones with Fast Charge Transfer for Perovskite Solar Cells. *Nano Energy* **2015**, *11*, 409–418.

(20) Li, X.; Dai, S. M.; Zhu, P.; Deng, L. L.; Xie, S. Y.; Cui, Q.; Chen, H.; Wang, N.; Lin, H. Efficient Perovskite Solar Cells Depending on TiO2 Nanorod Arrays. *ACS Appl. Mater. Interfaces* **2016**, *8* (33), 21358–21365.

(21) Salado, M.; Oliva-Ramirez, M.; Kazim, S.; González-Elipe, A. R.; Ahmad, S. 1-

Dimensional TiO2 Nano-Forests as Photoanodes for Efficient and Stable Perovskite Solar Cells Fabrication. *Nano Energy* **2017**, *35*, 215–222.

(22) Ramos, F. J.; Oliva-Ramirez, M.; Nazeeruddin, M. K.; Grätzel, M.; González-Elipe, A. R.; Ahmad, S. Nanocolumnar 1-Dimensional TiO 2 Photoanodes Deposited by PVD-OAD for Perovskite Solar Cell Fabrication. *J. Mater. Chem. A* **2015**, *3*, 13291–13298.

(23) Qin, P.; Paulose, M.; Dar, M. I.; Moehl, T.; Arora, N.; Gao, P.; Varghese, O. K.; Grätzel, M.; Nazeeruddin, M. K. Stable and Efficient Perovskite Solar Cells Based on Titania Nanotube Arrays. *Small* **2015**, *11* (41), 5533–5539.

(24) Jiang, Q.; Sheng, X.; Li, Y.; Feng, X.; Xu, T. Rutile TiO 2 Nanowire-Based Perovskite Solar Cells. *Chem. Commun.* **2014**, *50* (94), 14720–14723.

(25) Wu, S.; Chen, C.; Wang, J.; Xiao, J.; Peng, T. Controllable Preparation of Rutile TiO 2 Nanorod Array for Enhanced Photovoltaic Performance of Perovskite Solar Cells. *ACS Appl. Energy Mater.* **2018**, *1* (4), 1649–1657.

(26) Yang, H.-Y.; Rho, W.-Y.; Lee, S.; Kim, S.; Hahn, Y.-B. TiO2 Nanoparticles/Nanotubes for Efficient Light Harvesting in Perovskite Solar Cells. *Nanomaterials* **2019**, *9* (3), 326.

(27) Cui, Q.; Zhao, X.; Lin, H.; Yang, L.; Chen, H.; Zhang, Y.; Li, X. Improved Efficient Perovskite Solar Cells Based on Ta-Doped TiO2 Nanorod Arrays. *Nanoscale* **2017**, *9* (47), 18897–18907.

(28) Liu, C.; Zhu, R.; Ng, A.; Ren, Z.; Cheung, S. H.; Du, L.; So, S. K.; Zapien, J. A.; Djurišić, A. B.; Lee Phillips, D.; Surya, C. Investigation of High Performance TiO2 Nanorod Array Perovskite Solar Cells. *J. Mater. Chem. A* **2017**, *5* (30), 15970–15980.

(29) Gao, X.; Li, J.; Gollon, S.; Qiu, M.; Guan, D.; Guo, X.; Chen, J.; Yuan, C. A TiO 2 Nanotube Network Electron Transport Layer for High Efficiency Perovskite Solar Cells. *Phys. Chem. Chem. Phys.* **2017**, *19* (7), 4956–4961.

(30) Seo, M. S.; Jeong, I.; Park, J. S.; Lee, J.; Han, I. K.; Lee, W. I.; Son, H. J.; Sohn, B. H.; Ko, M. J. Vertically Aligned Nanostructured TiO2 Photoelectrodes for High Efficiency Perovskite Solar Cells: Via a Block Copolymer Template Approach. *Nanoscale* **2016**, *8* (22), 11472–11479.

(31) Zheng, L.; Ma, Y.; Chu, S.; Wang, S.; Qu, B.; Xiao, L.; Chen, Z.; Gong, Q.; Wu, Z.; Hou, X. Improved Light Absorption and Charge Transport for Perovskite Solar Cells with Rough Interfaces by Sequential Deposition. *Nanoscale* **2014**, *6* (14), 8171–8176.

(32) Pascoe, A. R.; Meyer, S.; Huang, W.; Li, W.; Benesperi, I.; Duffy, N. W.; Spiccia, L.; Bach, U.; Cheng, Y.-B. Enhancing the Optoelectronic Performance of Perovskite Solar Cells via a Textured CH 3 NH 3 PbI 3 Morphology. *Adv. Funct. Mater.* **2016**, *26* (8), 1278–1285.

(33) Shi, B.; Liu, B.; Luo, J.; Li, Y.; Zheng, C.; Yao, X.; Fan, L.; Liang, J.; Ding, Y.; Wei, C.; Zhang, D.; Zhao, Y.; Zhang, X. Enhanced Light Absorption of Thin Perovskite Solar Cells Using Textured Substrates. *Sol. Energy Mater. Sol. Cells* **2017**, *168*, 214–220.

(34) Jošt, M.; Albrecht, S.; Kegelmann, L.; Wolff, C. M.; Lang, F.; Lipovšek, B.; Krč, J.; Korte, L.; Neher, D.; Rech, B.; Topič, M. Efficient Light Management by Textured Nanoimprinted Layers for Perovskite Solar Cells. *ACS Photonics* **2017**, *4* (5), 1232–1239.

(35) Wang, D.-L.; Cui, H.-J.; Hou, G.-J.; Zhu, Z.-G.; Yan, Q.-B.; Su, G. Highly Efficient Light

Management for Perovskite Solar Cells. *Sci. Rep.* **2016**, *6* (1), 18922.

(36) Peer, A.; Biswas, R.; Park, J.-M.; Shinar, R.; Shinar, J. Light Management in Perovskite Solar Cells and Organic LEDs with Microlens Arrays. *Opt. Express* **2017**, *25* (9), 10704.

(37) Wang, H.; Cai, B.; Yuan, X. Significant Light Absorption Improvement in Perovskite/CIGS Tandem Solar Cells with Dielectric Nanocone Structures. *J. Phys. Conf. Ser.* **2017**, *844*, 012004.

(38) Luo, Q.; Zhang, C.; Deng, X.; Zhu, H.; Li, Z.; Wang, Z.; Chen, X.; Huang, S. Plasmonic Effects of Metallic Nanoparticles on Enhancing Performance of Perovskite Solar Cells. *ACS Appl. Mater. Interfaces* **2017**, *9* (40), 34821–34832.

(39) Ginting, R. T.; Kaur, S.; Lim, D.-K.; Kim, J.-M.; Lee, J. H.; Lee, S. H.; Kang, J.-W. Plasmonic Effect of Gold Nanostars in Highly Efficient Organic and Perovskite Solar Cells. *ACS Appl. Mater. Interfaces* **2017**, *9* (41), 36111–36118.

(40) Long, M.; Chen, Z.; Zhang, T.; Xiao, Y.; Zeng, X.; Chen, J.; Yan, K.; Xu, J. Ultrathin Efficient Perovskite Solar Cells Employing a Periodic Structure of a Composite Hole Conductor for Elevated Plasmonic Light Harvesting and Hole Collection. *Nanoscale* **2016**, *8* (12), 6290–6299.

(41) Yin, J.; Qu, H.; Cao, J.; Tai, H.; Li, J.; Zheng, N. Light Absorption Enhancement by Embedding Submicron Scattering TiO 2 Nanoparticles in Perovskite Solar Cells. *RSC Adv.* **2016**, *6* (29), 24596–24602.

(42) Haque, S.; Mendes, M. J.; Sanchez-Sobrado, O.; Águas, H.; Fortunato, E.; Martins, R. Photonic-Structured TiO2 for High-Efficiency, Flexible and Stable Perovskite Solar Cells.

Nano Energy **2019**, *59*, 91–101.

(43) Caldarola, M.; Albella, P.; Cortés, E.; Rahmani, M.; Roschuk, T.; Grinblat, G.; Oulton, R. F.; Bragas, A. V.; Maier, S. A. Non-Plasmonic Nanoantennas for Surface Enhanced Spectroscopies with Ultra-Low Heat Conversion. *Nat. Commun.* **2015**, *6* (1), 7915.

(44) Albella, P.; Poyli, M. A.; Schmidt, M. K.; Maier, S. A.; Moreno, F.; Sáenz, J. J.; Aizpurua, J. Low-Loss Electric and Magnetic Field-Enhanced Spectroscopy with Subwavelength Silicon Dimers. *J. Phys. Chem. C* **2013**, *117* (26), 13573–13584.

(45) Cambiasso, J.; Grinblat, G.; Li, Y.; Rakovich, A.; Cortés, E.; Maier, S. A. Bridging the Gap between Dielectric Nanophotonics and the Visible Regime with Effectively Lossless Gallium Phosphide Antennas. *Nano Lett.* **2017**, *17* (2), 1219–1225.

(46) Lin, H.-J.; de Oliveira Lima, K.; Gredin, P.; Mortier, M.; Billot, L.; Chen, Z.; Aigouy, L. Fluorescence Enhancement near Single TiO 2 Nanodisks. *Appl. Phys. Lett.* **2017**, *111* (25), 251109.

(47) Deniz, D.; Lad, R. J. Temperature Threshold for Nanorod Structuring of Metal and Oxide Films Grown by Glancing Angle Deposition. *J. Vac. Sci. Technol. A Vacuum, Surfaces, Film.* **2011**, *29* (1), 11020.

(48) Cansizoglu, M. F.; Engelken, R.; Seo, H. W.; Karabacak, T. High Optical Absorption of Indium Sulfide Nanorod Arrays Formed by Glancing Angle Deposition. *ACS Nano* **2010**, *4* (2), 733–740.

(49) Waita, S. M.; Aduda, B. O.; Mwabora, J. M.; Granqvist, C. G.; Lindquist, S. E.; Niklasson, G. A.; Hagfeldt, A.; Boschloo, G. Electron Transport and Recombination in Dye

Sensitized Solar Cells Fabricated from Obliquely Sputter Deposited and Thermally Annealed TiO2 Films. *J. Electroanal. Chem.* **2007**, *605* (2), 151–156.

(50) Bräuer, G.; Szyszka, B.; Vergöhl, M.; Bandorf, R. Magnetron Sputtering – Milestones of 30 Years. *Vacuum* **2010**, *84*, 1354–1359.

(51) Anders, A. Plasma and Ion Sources in Large Area Coating: A Review. *Surf. Coatings Technol.* **2005**, *200*, 1893–1906.

(52) Sanjinés, R.; Tang, H.; Berger, H.; Gozzo, F.; Margaritondo, G.; Lévy, F. Electronic Structure of Anatase TiO 2 Oxide. *J. Appl. Phys.* **1994**, *75* (6), 2945–2951.

(53) Ma, S.; Ahn, J.; Oh, Y.; Kwon, H.-C.; Lee, E.; Kim, K.; Yun, S.-C.; Moon, J. Facile Sol–Gel-Derived Craterlike Dual-Functioning TiO 2 Electron Transport Layer for High-Efficiency Perovskite Solar Cells. *ACS Appl. Mater. Interfaces* **2018**, *10* (17), 14649–14658.

(54) Bharti, B.; Kumar, S.; Lee, H.-N.; Kumar, R. Formation of Oxygen Vacancies and Ti3+ State in TiO2 Thin Film and Enhanced Optical Properties by Air Plasma Treatment. *Sci. Rep.* **2016**, *6* (1), 32355.

(55) Wang, Y.; Wu, J.; Zhang, P.; Liu, D.; Zhang, T.; Ji, L.; Gu, X.; David Chen, Z.; Li, S. Stitching Triple Cation Perovskite by a Mixed Anti-Solvent Process for High Performance Perovskite Solar Cells. *Nano Energy* **2017**, *39*, 616–625.

(56) Saliba, M.; Matsui, T.; Seo, J. Y.; Domanski, K.; Correa-Baena, J. P.; Nazeeruddin, M. K.; Zakeeruddin, S. M.; Tress, W.; Abate, A.; Hagfeldt, A.; Grätzel, M. Cesium-Containing Triple Cation Perovskite Solar Cells: Improved Stability, Reproducibility and High

Efficiency. *Energy Environ. Sci.* **2016**, *9* (6), 1989–1997.

(57) Chen, Q.; Zhou, H.; Song, T.-B.; Luo, S.; Hong, Z.; Duan, H.-S.; Dou, L.; Liu, Y.; Yang, Y. Controllable Self-Induced Passivation of Hybrid Lead Iodide Perovskites toward High Performance Solar Cells. *Nano Lett.* **2014**, *14* (7), 4158–4163.

(58) Zhang, H.; Li, Y.; Ivanov, I. A.; Qu, Y.; Huang, Y.; Duan, X. Plasmonic Modulation of the Upconversion Fluorescence in NaYF 4: Yb/Tm Hexaplate Nanocrystals Using Gold Nanoparticles or Nanoshells. *Angew. Chemie - Int. Ed.* **2010**, *49* (16), 2865–2868.

(59) Wang, P. H.; Li, Z. Q.; Salcedo, W. J.; Sun, Z.; Huang, S. M.; Brolo, A. G. Surface Plasmon Enhanced Up-Conversion from NaYF4:Yb/Er/Gd Nano-Rods. *Phys. Chem. Chem. Phys.* **2015**, *17* (24), 16170–16177.

(60) Aigouy, L.; González, M.-U.; Lin, H.-J.; Schoenauer-Sebag, M.; Billot, L.; Gredin, P.; Mortier, M.; Chen, Z.; García-Martín, A. Mapping Plasmon-Enhanced Upconversion Fluorescence of Er/Yb-Doped Nanocrystals near Gold Nanodisks. *Nanoscale* **2019**, *11* (21), 10365–10371.

(61) Feng, J.; Zhu, X.; Yang, Z.; Zhang, X.; Niu, J.; Wang, Z.; Zuo, S.; Priya, S.; Liu, S. (Frank); Yang, D. Record Efficiency Stable Flexible Perovskite Solar Cell Using Effective Additive Assistant Strategy. *Adv. Mater.* **2018**, *30* (35), 1801418.

(62) Hu, W.; Zhou, W.; Lei, X.; Zhou, P.; Zhang, M.; Chen, T.; Zeng, H.; Zhu, J.; Dai, S.; Yang, S.; Yang, S. Low-Temperature In Situ Amino Functionalization of TiO 2 Nanoparticles Sharpens Electron Management Achieving over 21% Efficient Planar Perovskite Solar Cells. *Adv. Mater.* **2019**, *31*, 1806095.

(63) Alvarez, R.; Garcia-Martin, J. M.; Garcia-Valenzuela, A.; Macias-Montero, M.; Ferrer, F. J.; Santiso, J.; Rico, V.; Cotrino, J.; Gonzalez-Elipe, A. R.; Palmero, A. Nanostructured Ti Thin Films by Magnetron Sputtering at Oblique Angles. *J. Phys. D. Appl. Phys.* **2016**, *49*, 045303.

(64) Edri, E.; Kirmayer, S.; Cahen, D.; Hodes, G. High Open-Circuit Voltage Solar Cells Based on Organic-Inorganic Lead Bromide Perovskite. *J. Phys. Chem. Lett.* **2013**, *4*, 897–902.

(65) Chen, H.; Zheng, X.; Li, Q.; Yang, Y.; Xiao, S.; Hu, C.; Bai, Y.; Zhang, T.; Wong, K. S.; Yang, S. An Amorphous Precursor Route to the Conformable Oriented Crystallization of Ch3nh3pbbr3 in Mesoporous Scaffolds: Toward Efficient and Thermally Stable Carbon-Based Perovskite Solar Cells. *J. Mater. Chem. A* **2016**, *4* (33), 12897–12912.

(66) Hu, Z.; Xiang, H.; Schoenauer Sebag, M.; Billot, L.; Aigouy, L.; Chen, Z. Compact Layer Free Mixed-Cation Lead Mixed-Halide Perovskite Solar Cells. *Chem. Commun.* **2018**, *54*, 2623–2626.

(67) Mahboubi Soufiani, A.; Yang, Z.; Young, T.; Miyata, A.; Surrente, A.; Pascoe, A.; Galkowski, K.; Abdi-Jalebi, M.; Brenes, R.; Urban, J.; Zhang, N.; Bulović, V.; Portugall, O.; Cheng, Y.-B.; Nicholas, R. J.; Ho-Baillie, A.; Green, M. A.; Plochocka, P.; Stranks, S. D. Impact of Microstructure on the Electron–Hole Interaction in Lead Halide Perovskites. *Energy Environ. Sci.* **2017**, *10*, 1358–1366.

(68) Aigouy, L.; González, M.-U.; Lin, H.-J.; Schoenauer-Sebag, M.; Billot, L.; Gredin, P.; Mortier, M.; Chen, Z.; García-Martín, A. Mapping Plasmon-Enhanced Upconversion Fluorescence of Er/Yb-Doped Nanocrystals near Gold Nanodisks. *Nanoscale* **2019**, *11* (21), 10365–10371.

(69) Lin, H.-J.; de Oliveira Lima, K.; Gredin, P.; Mortier, M.; Billot, L.; Chen, Z.; Aigouy, L. Fluorescence Enhancement near Single TiO2 Nanodisks. *Appl. Phys. Lett.* **2017**, *111* (25), 251109.

TOC Graphic